

# Horizontal Line Nodes in $\text{Sr}_2\text{RuO}_4$ Proved by Spin Resonance

Kazuki Iida,<sup>1,2,\*</sup> Maiko Kofu,<sup>1,3</sup> Katsuhiko Suzuki,<sup>4</sup> Naoki Murai,<sup>3</sup> Ryoichi Kajimoto,<sup>3</sup> Seiko Ohira-Kawamura,<sup>3</sup> Yasuhiro Inamura,<sup>3</sup> Motoyuki Ishikado,<sup>2</sup> Shunsuke Hasegawa,<sup>5</sup> Takatsugu Masuda,<sup>5</sup> Yoshiyuki Yoshida,<sup>6</sup> Kazushige Machida,<sup>7</sup> and Seunghun Lee<sup>1</sup>

<sup>1</sup>*Department of Physics, University of Virginia, Charlottesville, Virginia 22904-4714, USA*

<sup>2</sup>*Neutron Science and Technology Center, Comprehensive Research*

*Organization for Science and Society (CROSS), Tokai, Ibaraki 319-1106, Japan*

<sup>3</sup>*J-PARC Center, Japan Atomic Energy Agency (JAEA), Tokai, Ibaraki 319-1195, Japan*

<sup>4</sup>*Research Organization of Science and Technology,*

*Ritsumeikan University, Kusatsu, Shiga 525-8577, Japan*

<sup>5</sup>*Neutron Science Laboratory, Institute for Solid State Physics,*

*University of Tokyo, Kashiwa, Chiba 277-8581, Japan*

<sup>6</sup>*National Institute of Advanced Industrial Science and Technology, Tsukuba, Ibaraki 305-8565, Japan*

<sup>7</sup>*Department of Physics, Ritsumeikan University, Kusatsu, Shiga 525-8577, Japan*

(Dated: April 9, 2020)

We investigated the low-energy incommensurate (IC) magnetic fluctuations in  $\text{Sr}_2\text{RuO}_4$  by the high-resolution inelastic neutron scattering measurements and random phase approximation (RPA) calculations. We observed a spin resonance with energy of  $\hbar\omega_{\text{res}} = 0.56$  meV centered at a characteristic wavevector  $\mathbf{Q}_{\text{res}} = (0.3, 0.3, 0.5)$ . The resonance energy corresponds well to the superconducting gap  $2\Delta = 0.56$  meV estimated by the tunneling spectroscopy. The spin resonance shows the  $L$  modulation with a maximum at around  $L = 0.5$ . The  $L$  modulated intensity of the spin resonance and our RPA calculations indicate that the superconducting gaps regarding the quasi-one-dimensional  $\alpha$  and  $\beta$  sheets at the Fermi surfaces have the horizontal line nodes. These results may set a strong constraint on the pairing symmetry of  $\text{Sr}_2\text{RuO}_4$ . We also discuss the implications on possible superconducting order parameters.

Strontium ruthenate  $\text{Sr}_2\text{RuO}_4$  with  $T_c = 1.5$  K<sup>1</sup> has attracted a great deal of interest as a prime candidate for the chiral  $p$ -wave superconductor<sup>2-5</sup>; nuclear magnetic resonance (NMR)<sup>6</sup> and polarized neutron scattering<sup>7</sup> measurements reported spin-triplet superconductivity whereas muon spin rotation<sup>8</sup> and Kerr effect<sup>9</sup> measurements showed spontaneously time reversal symmetry breaking. On the other hand, there are some experimental results such as the absence of the chiral edge currents<sup>10</sup>, first-order superconducting transition<sup>11-14</sup>, and strong  $H_{c2}$  ( $\parallel ab$ ) suppression<sup>15</sup>, all of which challenge the chiral  $p$ -wave superconductivity. Recently, experimental and theoretical studies under an application of uniaxial pressure along  $\langle 100 \rangle$  reported a factor of 2.3 enhancement of  $T_c$  owing to the Lifshitz transition when the Fermi level passes through a van Hove singularity, raising the possibility of an even-parity spin-singlet order parameter in  $\text{Sr}_2\text{RuO}_4$ <sup>16-22</sup>. More recently, new NMR results demonstrated that the spin susceptibility substantially drops below  $T_c$  provided that the pulse energy is smaller than a threshold, ruling out the chiral- $p$  spin-triplet superconductivity<sup>23,24</sup>. As such, these recent works turn the research on  $\text{Sr}_2\text{RuO}_4$  towards a fascinating new era.

So far, various experimental techniques reported that the superconducting gaps of  $\text{Sr}_2\text{RuO}_4$  have line nodes<sup>25,26</sup>, but the details of the line nodes, e.g. of the vertical or horizontal nature, are not uncovered yet. The thermal conductivity measurements reported vertical line nodes on the superconducting gaps<sup>27</sup>, whereas field-angle-dependent specific heat capacity measurements are indicating the horizontal line nodes<sup>28,29</sup>. Since the com-

plete information of the superconducting gaps can shed light on the symmetry of the pairing, exclusive determination of the direction of the line nodes in  $\text{Sr}_2\text{RuO}_4$  is highly desirable.

The inelastic neutron scattering (INS) technique can directly measure the imaginary part of generalized spin susceptibility ( $\chi''$ ) as a function of momentum ( $\mathbf{Q}$ ) and energy ( $\hbar\omega$ ) transfers, yielding information on the Fermi surface topology. In addition,  $\mathbf{Q}$  dependence of a spin resonance as a consequence of the Bardeen-Cooper-Schrieffer (BCS) coherence factor can provide information on the symmetry of the superconducting gap. In  $\text{Sr}_2\text{RuO}_4$ , the most pronounced magnetic signal in the normal state is nearly two-dimensional incommensurate (IC) magnetic fluctuations at  $\mathbf{Q}_{\text{IC}} = (0.3, 0.3, L)$  owing to the Fermi surface nesting between (or within) the quasi-one-dimensional  $\alpha$  and  $\beta$  sheets consisted of the  $d_{zx}$  and  $d_{yz}$  orbitals of Ru<sup>4+</sup><sup>30-33</sup>. In contrast to the marked signal from the IC magnetic fluctuations, only weak signals due to ferromagnetic fluctuations originating from the two-dimensional  $\gamma$  sheet ( $d_{xy}$ ) are observed around the  $\Gamma$  point<sup>34,35</sup>. Upon decreasing temperature below  $T_c$ , however, no sizable spin resonance regarding the IC magnetic fluctuations<sup>36</sup> was observed at  $\mathbf{Q} = (0.3, 0.3, 0)$  with energy close to the superconducting gap  $2\Delta = 0.56$  meV<sup>33</sup> estimated by the tunneling spectroscopy<sup>37</sup>.

Based on the horizontal line nodes model, the spin resonance is supposed to emerge at  $\mathbf{Q} = (0.3, 0.3, L)$  with a finite  $L$  but not at  $(0.3, 0.3, 0)$  because of the sign change of the superconducting gap along  $k_z$ <sup>29</sup>. The vertical line nodes model, on the other hand, expects the spin res-

onance at  $\mathbf{Q} = (0.3, 0.3, 0)$  because of the sign change within the  $k_z$  plane. Therefore, the horizontal line nodes model can naturally explain the absence of the spin resonance at  $\mathbf{Q} = (0.3, 0.3, 0)$ , and search for the spin resonance at  $(0.3, 0.3, L)$  is of particular interest. In this letter, we investigate in detail the low-energy IC magnetic fluctuations in  $\text{Sr}_2\text{RuO}_4$  focusing on their  $L$  dependence using the high-resolution INS technique. The experimental results, especially the  $L$  dependence of neutron scattering intensities, are compared with the random phase approximation (RPA) calculations.

Three single crystals of  $\text{Sr}_2\text{RuO}_4$  with a total mass of  $\sim 10$  g were grown by the floating-zone method<sup>38,39</sup>, and each crystal shows the superconducting onset temperature of  $\sim 1.35$  K. They were co-aligned with the  $(HHL)$  plane being horizontal to the scattering plane and attached to a closed-cycle  $^3\text{He}$  refrigerator. We performed INS measurements at 0.3 and 1.8 K using the disk chopper time-of-flight (TOF) neutron spectrometer AMATERAS of the Materials and Life Science Experimental Facility (MLF) in Japan Proton Accelerator Research Complex (J-PARC)<sup>40</sup>. Frequency of the pulse shaping and velocity selecting disk choppers was 300 Hz, yielding the combinations of multiple incident neutron energies ( $E_i$ s) of 2.64, 5.93, and 23.7 meV with the energy resolutions of 0.046, 0.146, and 1.07 meV, respectively, at the elastic channel. The software suite Utsusemi<sup>41</sup> was used to visualize the TOF neutron scattering data.

Figure 1 summarizes the overall features of high-energy ( $\hbar\omega \gg 2\Delta$ ) IC magnetic fluctuations with  $L = 0.5$  in  $\text{Sr}_2\text{RuO}_4$ . Figure 1(a) depicts the constant-energy INS intensity map in the  $(HK0.5)$  plane with energy transfer of 2.5 meV at 0.3 K. IC magnetic fluctuations are observed at  $\mathbf{Q}_{\text{IC}} = (0.3, 0.3, 0.5)$ ,  $(0.7, 0.3, 0.5)$ , and  $(0.7, 0.7, 0.5)$ . In addition to the IC magnetic fluctuations, the Fermi surface nesting also induces the ridge scattering connecting equivalent  $\mathbf{Q}_{\text{IC}}$ s around  $(0.5, 0.5, 0.5)$ . To explore the energy evolution of the IC magnetic fluctuations with  $L = 0.5$ , the INS intensity is converted to the imaginary part of the spin susceptibility  $\chi''(\hbar\omega)$  via the fluctuation-dissipation theorem  $\chi''(\hbar\omega) = (1 - e^{-\hbar\omega/k_B T})I(\hbar\omega)$  after subtracting the background. The  $\chi''(\hbar\omega)$  spectra at  $\mathbf{Q}_{\text{IC}} = (0.3, 0.3, 0.5)$  below and above  $T_c$  are plotted in Fig. 1(c). The  $\chi''(\hbar\omega)$  spectra above 1.0 meV are well fitted by the relaxation response model  $\chi''(\hbar\omega) = \chi' \Gamma \hbar\omega / [(\hbar\omega)^2 + \Gamma^2]$  where  $\chi'$  is the static susceptibility and  $\Gamma$  the relaxation rate [or the peak position of  $\chi''(\hbar\omega)$ ], yielding  $\Gamma = 6.3(2)$  meV [ $6.5(2)$  meV] at 0.3 K (1.8 K). The observed IC magnetic fluctuations with  $L = 0.5$  are quantitatively consistent with the IC magnetic fluctuations with  $L = 0$  reported in the previous INS works<sup>31–35</sup>. This is reasonable since the IC magnetic fluctuations along  $(0.3, 0.3, L)$  monotonically decrease in intensity with increasing  $L$  [Fig. 1(b)], representing the quasi-two-dimensional nature of the IC magnetic fluctuations in this energy region. This is consistent with the quasi-one-dimensional band structures of the cylindrical  $\alpha$  and  $\beta$  sheets<sup>42</sup>.

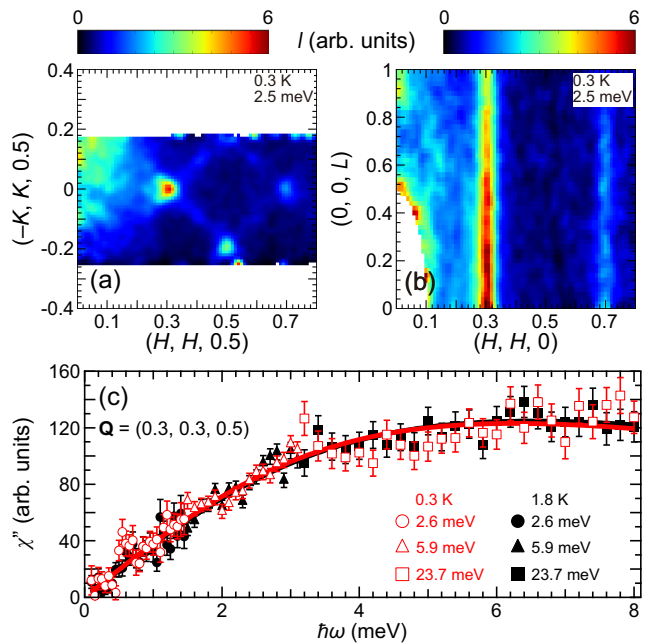


FIG. 1. (Color online) High-energy INS results of the IC magnetic fluctuations in  $\text{Sr}_2\text{RuO}_4$ . (a, b) Constant-energy INS intensity maps in the (a)  $(HK0.5)$  and (b)  $(HHL)$  planes with the energy window of  $[1.5, 3.5]$  meV at 0.3 K. (c)  $\chi''(\hbar\omega)$  spectra at  $\mathbf{Q}_{\text{IC}} = (0.3, 0.3, 0.5)$  below and above  $T_c$ . Data from different incident energies of neutrons  $E_i = 2.64, 5.93,$  and  $23.7$  meV (circles, triangles, and squares) are combined for each temperature after background estimated by  $\chi''(\hbar\omega)$  at  $\mathbf{Q} = (0.525, 0.525, 0.5)$  is subtracted from each spectrum. Solid lines are fitting results by the conventional relaxation response model.

Let us turn to the low-energy ( $\hbar\omega \simeq 2\Delta$ ) IC magnetic fluctuations of  $\text{Sr}_2\text{RuO}_4$ . We found that a spin resonance appears in the superconducting state at  $\mathbf{Q}_{\text{res}} = (0.3, 0.3, 0.5)$  and  $\hbar\omega_{\text{res}} = 2\Delta$  [white arrow in Fig. 2(a)] but not at  $\mathbf{Q} = (0.3, 0.3, 0)$  [Fig. 2(c)]. The  $L$  modulated intensity of the spin resonance is observed only at  $\hbar\omega = 2\Delta$  [Fig. 2(e)]. The intensity modulation along  $L$  of the low-energy IC magnetic fluctuations indicates the presence of a weakly three-dimensional superconducting gaps. It is worth mentioning that the low-energy magnetic fluctuations at  $\mathbf{Q} = (0.7, 0.7, L)$  is difficult to detect in this low-energy region because of the quickly decaying squared magnetic form factor at high  $Q$  [ $F_{\mathbf{Q}=(0.7,0.7,0.5)}^2 / F_{\mathbf{Q}=(0.3,0.3,0.5)}^2 \sim 1/6^{43}$ ] and the weak intensity of the IC magnetic fluctuations at low energies [Fig. 1(c)]. For quantitative analysis on the spin resonance in  $\text{Sr}_2\text{RuO}_4$ ,  $\hbar\omega$  and  $\mathbf{Q}$  dependencies of the INS intensity [ $I(\hbar\omega)$  and  $I(\mathbf{Q})$ ] are analyzed in detail below.

$I(\hbar\omega)$  cuts at  $\mathbf{Q} = (0.3, 0.3, 0.5)$  and  $(0.3, 0.3, 0)$  are plotted in Figs. 3(a) and 3(b), respectively. Below  $T_c$ , a clear increment in intensity at  $\hbar\omega \sim 0.56$  meV can be seen in the  $I(\hbar\omega)$  cut at  $(0.3, 0.3, 0.5)$  [shaded area in Fig. 3(a)]. Meanwhile, such enhancement at  $\hbar\omega \sim 0.56$  meV below  $T_c$  is not observed in the  $I(\hbar\omega)$

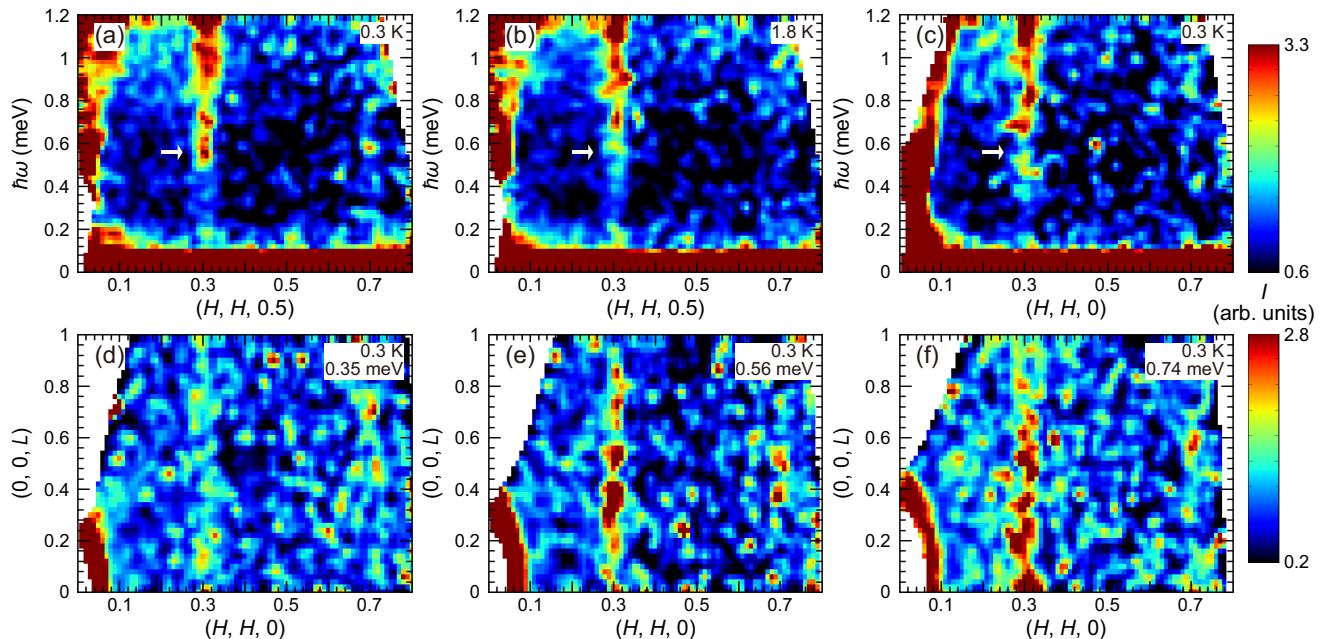


FIG. 2. (Color online) Low-energy INS intensity maps regarding the IC magnetic fluctuations in  $\text{Sr}_2\text{RuO}_4$ . (a–c) Low-energy IC magnetic fluctuations (a) along  $\mathbf{Q} = (H, H, 0.5)$  at 0.3 K, (b) along  $(H, H, 0.5)$  at 1.8 K, and (c) along  $(H, H, 0)$  at 0.3 K. White arrows indicate the energy of the superconducting gap  $2\Delta$  at  $\mathbf{Q}_{\text{IC}}$ . (d–f) Constant-energy INS intensity maps in the  $(HHL)$  plane at 0.3 K with the energy windows of (d) [0.23, 0.47] meV, (e) [0.47, 0.65] meV, and (f) [0.65, 0.83] meV.

cut at  $(0.3, 0.3, 0)$  [Fig. 3(b)], consistent with the previous INS study<sup>33</sup>.  $I(\mathbf{Q})$  cuts at  $\hbar\omega = 0.56$  meV along  $\mathbf{Q} = (H, H, 0.5)$  and  $(H, H, 0)$  also show the same trend [Figs. 3(c) and 3(d)]. The IC fluctuations at  $\hbar\omega = 0.56$  meV along  $\mathbf{Q} = (H, H, 0.5)$  are enhanced below  $T_c$  [shaded area in Fig. 3(c)], while the IC fluctuations at  $\hbar\omega = 0.56$  meV along  $\mathbf{Q} = (H, H, 0)$  do not change in intensity across  $T_c$  [Fig. 3(d)]. Figure 3(e) shows the  $I(\mathbf{Q})$  cuts along  $\mathbf{Q} = (H, H, 0.5)$  for three different energies,  $\hbar\omega = 0.35, 0.56,$  and  $0.74$  meV. The  $I(\mathbf{Q})$  cuts exhibit peaks centered at  $\mathbf{Q}_{\text{IC}} = (0.3, 0.3, 0.5)$  owing to the IC magnetic fluctuations in all the energy windows at both temperatures. Interestingly, only the INS intensity at  $\hbar\omega = 0.56$  meV shows sizable enhancement at  $\mathbf{Q}_{\text{IC}}$  in the superconducting state compared to the normal state [shaded area in Fig. 3(e)]. We emphasize that the energy,  $\hbar\omega = 0.56$  meV, corresponds well to the superconducting gap  $2\Delta$ <sup>37</sup> [vertical bar in Fig. 3(a)], suggesting that the observed enhancement, localized in both  $\mathbf{Q}_{\text{res}} = (0.3, 0.3, 0.5)$  and  $\hbar\omega_{\text{res}} = 0.56$  meV, is the spin resonance [see also white arrow in Fig. 2(a)]. The spin gap of the IC magnetic fluctuations at  $\mathbf{Q}_{\text{IC}} = (0.3, 0.3, 0.5)$  is smaller than 0.2 meV [Fig. 3(a)], which makes the spin resonance less pronounced.  $I(\mathbf{Q})$  cuts at 0.74 meV in Fig. 3(e) also shows a tiny increment at 0.3 K. A possible scenario is that the reported superconducting gap value<sup>37</sup> is band averaged and the superconducting gaps regarding the  $\alpha$  and  $\beta$  bands are slightly larger than  $2\Delta = 0.56$  meV.

$L$  dependence of the low-energy IC magnetic fluctuations can provide us a compelling evidence to clarify the nodal nature of the superconducting gaps<sup>29</sup>. Fig-

ures 2(d)–2(f) illustrate contour maps of the INS intensities in the  $(HHL)$  plane at 0.3 K with the energies 0.35, 0.56, and 0.74 meV, and  $I(\mathbf{Q})$  cuts along  $\mathbf{Q} = (0.3, 0.3, L)$  at 0.3 K with the corresponding energies are also plotted in Fig. 3(f). In contrast to the monotonically decreasing intensities of the IC magnetic fluctuations at 0.35 and 0.74 meV following the squared magnetic form factor of  $\text{Sr}_2\text{RuO}_4$ <sup>43</sup> [the dashed lines in Fig. 3(f)], the  $I(\mathbf{Q})$  cut at the spin resonance energy (0.56 meV) shows a maximum at  $L \sim 0.5$  besides the monotonically decreasing component of the IC magnetic fluctuations [the shaded area and the dashed line in Fig. 3(f)]. The  $L$  modulated spin resonance represents the gap symmetry as the feedback effect from the superconducting gaps. Also, the  $L$  modulated intensity explains the absence of the spin resonance at  $\mathbf{Q} = (0.3, 0.3, 0)$  [Figs. 2(c), 3(b), and 3(d)]. To theoretically elucidate the origin of the  $L$  modulated intensity of the spin resonance in  $\text{Sr}_2\text{RuO}_4$ , RPA calculations assuming the horizontal line nodes at the superconducting gaps were further performed.

To construct a realistic model, we perform density functional theory (DFT) calculations using the Wien2k package<sup>44</sup>. We obtain an effective 3-orbital model considering the Ru  $d_{xz}, d_{yz}, d_{xy}$ -orbitals using the maximum localized Wannier functions<sup>45</sup>. The generalized gradient approximation (GGA) exchange-correlation functional<sup>46</sup> is adopted with the cut-off energy  $RK_{\text{max}} = 7$  and 512  $k$ -point mesh. We renormalize the bandwidth considering the effective mass  $m^* = 3.5$ , and the resulting renormalized bandwidth is  $W \sim 1.05$  eV. We consider the

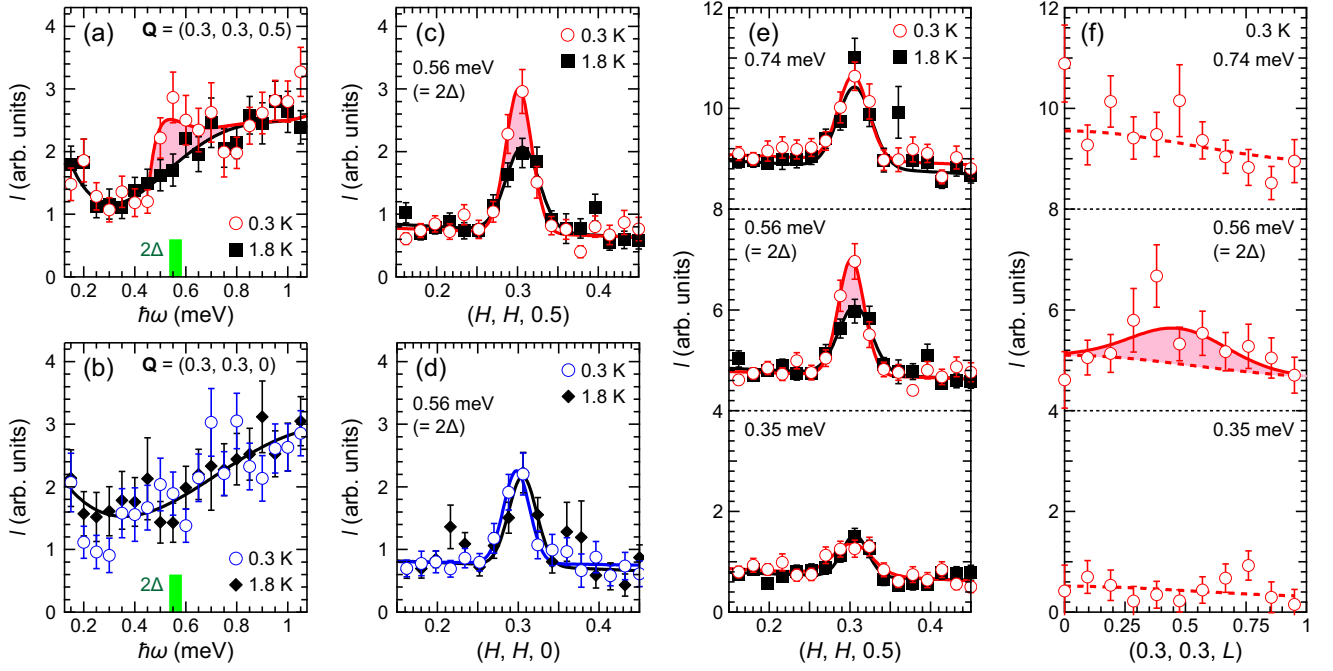


FIG. 3. (Color online)  $I(\hbar\omega)$  and  $I(\mathbf{Q})$  cuts of the low-energy IC magnetic fluctuations in  $\text{Sr}_2\text{RuO}_4$ . (a, b)  $I(\hbar\omega)$  cuts at (a)  $\mathbf{Q} = (0.3, 0.3, 0.5)$  and (b)  $(0.3, 0.3, 0)$  below and above  $T_c$ . Solid lines are the guides for the eye. Vertical bars represent the superconducting gap  $2\Delta = 0.56 \text{ meV}$ <sup>37</sup>. (c, d)  $I(\mathbf{Q})$  cuts along (c)  $\mathbf{Q} = (H, H, 0.5)$  and (d)  $(H, H, 0)$  at 0.3 and 1.8 K with the energy window of  $[0.47, 0.65] \text{ meV}$ . Solid lines are the fitting results by the Gaussian function with linear background. (e)  $I(\mathbf{Q})$  cuts along  $\mathbf{Q} = (H, H, 0.5)$  at 0.3 and 1.8 K with the energy windows of  $[0.23, 0.47]$ ,  $[0.47, 0.65]$ , and  $[0.65, 0.83] \text{ meV}$ . Solid lines are the fitting results. (f)  $I(\mathbf{Q})$  cuts along  $\mathbf{Q} = (0.3, 0.3, L)$  at 0.3 K with the energy windows of  $[0.23, 0.47]$ ,  $[0.47, 0.65]$ , and  $[0.65, 0.83] \text{ meV}$ . Background estimated by  $I(\mathbf{Q})$  along  $\mathbf{Q} = (0.525, 0.525, L)$  at 0.3 K is subtracted from each spectrum. Dashed lines are the squared magnetic form factor of  $\text{Sr}_2\text{RuO}_4$ <sup>43</sup> and therefore represent the components of the nearly two-dimensional IC magnetic fluctuations. The solid line is the guides for the eye. Shaded areas in panels (a, c, e, f) indicate the spin resonance.

following gap function with horizontal line nodes:

$$\Delta(\mathbf{k}) = \Delta_0 \cos ck_z \quad (1)$$

within the standard BCS framework. We take the gap amplitude  $\Delta_0 = 4.8 \times 10^{-3}W$ . In the body center tetragonal system, the period along to the  $k_z$  axis is  $4\pi/c$ , and thus we take  $k_z$  as  $0 \leq k_z < 4\pi/c$ . We obtain the dynamical spin susceptibility  $\chi_s^{\text{total}}(\mathbf{q}, \omega)$  applying RPA as

$$\chi_s^{\text{total}}(\mathbf{q}, \omega) = \sum_{l,m} \chi_s^{l,l,m,m}(\mathbf{q}, \omega) \quad (2)$$

$$\hat{\chi}_s(\mathbf{q}, \omega) = \hat{\chi}_0(\mathbf{q}, \omega) [\hat{I} - \hat{S}\hat{\chi}_0(\mathbf{q}, \omega)]^{-1} \quad (3)$$

$$\hat{\chi}_0(\mathbf{q}, \omega) = \hat{\chi}_{0,G}(\mathbf{q}, \omega) + \hat{\chi}_{0,F}(\mathbf{q}, \omega) \quad (4)$$

$$\chi_{0,G(F)}^{l_1, l_2, l_3, l_4}_{\sigma_1, \sigma_2, \sigma_3, \sigma_4}(\mathbf{q}, \omega) = \sum_k \sum_{n,m} \frac{f(E_{\mathbf{k}+\mathbf{q}}^n) - f(E_{\mathbf{k}}^m)}{\omega + i\delta - E_{\mathbf{k}+\mathbf{q}}^n + E_{\mathbf{k}}^m} \times U_{l_1, \sigma_1, n}(\mathbf{k} + \mathbf{q}) U_{l_4, \sigma_4, m}(\mathbf{k}) \times U_{m, l_2, \sigma_2}^\dagger(\mathbf{k}) U_{n, l_3, \sigma_3}^\dagger(\mathbf{k} + \mathbf{q}) \quad (5)$$

where  $l_1 \sim l_4$  and  $\sigma_1 \sim \sigma_4$  are the orbital ( $d_{xz}, d_{yz}, d_{xy}$ ) and spin ( $\uparrow$  and  $\downarrow$ ) indices.  $\hat{\chi}_{0,G(F)}$  denotes the normal

(anomalous) part of the irreducible bare susceptibility  $\hat{\chi}_0$  at  $\sigma_1 = \sigma_2 = \sigma_3 = \sigma_4$  ( $\sigma_1 = \sigma_2 \neq \sigma_3 = \sigma_4$ ).  $E_{\mathbf{k}}^n$  and  $f(E_{\mathbf{k}}^n)$  are the eigenvalue and Fermi distribution function of Bogoliubov quasi-particles.  $\hat{S}$  is the interaction vertex matrix<sup>47</sup>. We consider the on-site intra- and inter-orbital Coulomb interactions  $U_l$  and  $U'$  as  $U_{dxz/dyz} = 0.21W$ ,  $U_{dxy} = 0.7U_{dxz/dyz}$ ,  $U' = 3U_{dxz/dyz}/4$ . The Hund's coupling and pair hopping  $J = J' = U_{dxz/dyz}/8$ . We take the temperature  $T = 1.9 \times 10^{-3}W$ , the smearing factor  $\delta = 1.9 \times 10^{-3}W$  and  $1024 \times 1024 \times 32$   $k$ -mesh. The resulting characteristic spectral features of the dynamical spin susceptibility are not much influenced by the detailed parameter values mentioned above.

Figures 4(a) and 4(b) illustrate the calculated dynamical spin susceptibilities for energies,  $\hbar\omega = 2\Delta_0$  and  $4\Delta_0$ . We note that our calculations do not include the squared magnetic form factor of  $\text{Sr}_2\text{RuO}_4$  for clear visualization of the  $L$  dependence. For  $\hbar\omega = 2\Delta_0$ , the dynamical spin susceptibility shows the maximum at  $\mathbf{Q} = (1/3, 1/3, 1/2)$  and  $(2/3, 2/3, 1/2)$  as illustrated in Fig. 4(a). The superconducting gaps with the horizontal line nodes described in Eq. (1) give such the feature along  $L$ , which is indeed observed in our INS measurements [Fig. 2(e)]. We address that the observed  $L$  modulated intensity cannot be explained by the superconducting gap with the ver-

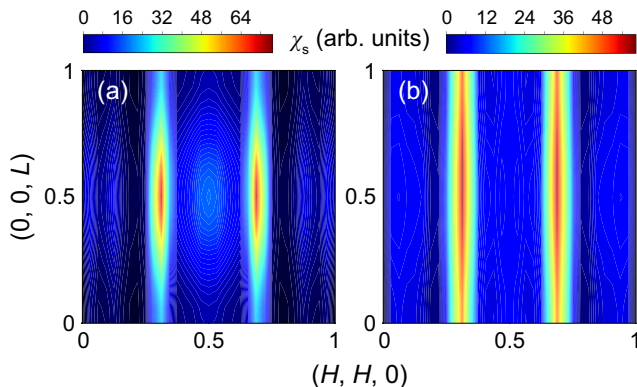


FIG. 4. (Color online) Calculated density maps of the dynamical spin susceptibility assuming the horizontal line nodes in  $\text{Sr}_2\text{RuO}_4$ . (a)  $\hbar\omega = 2\Delta_0$ . (b)  $\hbar\omega = 4\Delta_0$ .

tical line nodes since the superconducting gap changes its sign within the  $k_z$  plane<sup>29</sup>. On the other hand, no pronounced  $L$  modulation at higher energy transfers is observed either in the experiment [Fig. 2(f)], except the monotonically decreasing intensities due to the magnetic form factor, or in the calculation [Fig. 4(b)]. Since the energy window is too high compared to the superconducting gaps in  $\text{Sr}_2\text{RuO}_4$ <sup>37</sup>, the effect of the superconducting gaps smears out, and only the quasi-two-dimensional feature of the IC magnetic fluctuations show up in the higher energy windows ( $\hbar\omega \gg 2\Delta$ ).

The observed spin resonance at  $\mathbf{Q}_{\text{res}} = (0.3, 0.3, 0.5)$  and  $\hbar\omega_{\text{res}} = 2\Delta$  indicates that the quasi-one-dimensional  $\alpha$  and  $\beta$  sheets are active bands for the bulk superconductivity of  $\text{Sr}_2\text{RuO}_4$ . Our RPA calculations reveal that the observed  $L$  modulated intensity of the spin resonance originates from the horizontal line nodes at the superconducting gaps, in agreement with the field-angle-dependent specific heat capacity measurements<sup>12</sup>. We believe that our results give a strong constraint on the superconducting pairing symmetry of  $\text{Sr}_2\text{RuO}_4$ .

Let us now discuss the possible pairing symmetry of  $\text{Sr}_2\text{RuO}_4$ . Among the pairing symmetries with the horizontal line nodes proposed by the recent uniaxial pressure<sup>16–22</sup> and NMR works<sup>23,24</sup>, the chiral  $d$ -wave  $(k_x + ik_y)k_z$ <sup>48</sup> is compatible with the time-reversal sym-

metry breaking<sup>8,9</sup>. However, its wave function is odd in the  $k_z$  plane giving rise to the spin resonance at  $\mathbf{Q} = (0.3, 0.3, 0)$ , and thus such pairing symmetry can be excluded by our INS data. Recently, the Josephson effects measurements suggested the time-reversal invariant superconductivity in  $\text{Sr}_2\text{RuO}_4$ <sup>49</sup>. Combined with the time-reversal invariant superconductivity and the horizontal line nodes,  $d$ -wave  $d_{3k_z^2-1}$ <sup>29</sup> is proposed for the candidate for the pairing symmetry of  $\text{Sr}_2\text{RuO}_4$ . The single component order parameter is also in line with the absence of a split transition in the presence of uniaxial strain and  $T_c$  cusp in the limit of zero strain<sup>16–18</sup>. We note that the horizontal line nodes assuming  $d_{3k_z^2-1}$  is not symmetry protected. However, the horizontal line nodes can be realized even if the  $d$ -wave  $d_{3k_z^2-1}$  belonging to the  $A_{1g}$  representation in the point group  $D_{4h}$  slightly mixes with the  $s$  wave. Here, we emphasize that the spin resonance at  $L = 0.5$  is more sensitive to the gap modulation along  $k_z$  than the  $k_z$  position of horizontal line nodes. The candidate of the origin of the horizontal nodes is a competition of pairing mechanisms. Since spin fluctuations are highly two-dimensional, it would be difficult to arise three-dimensional gap structure only with pure spin fluctuation mechanism. The crystal structure of  $\text{Sr}_2\text{RuO}_4$  is body-centered tetragonal. Therefore, it seems that the electron-phonon<sup>50</sup> mediated mechanism would have three-dimensionality. The observed weakly three-dimensional spin resonance at  $L = 0.5$  may come from a competition between spin fluctuations and electron-phonon coupling.

In summary, we investigated the low-energy IC magnetic fluctuations in  $\text{Sr}_2\text{RuO}_4$  below and above  $T_c$  with detailed analysis on the  $L$  dependence. Below  $T_c$ , the spin resonance appears at  $\mathbf{Q}_{\text{res}} = (0.3, 0.3, 0.5)$  and  $\hbar\omega_{\text{res}} = 0.56$  meV. The spin resonance shows the  $L$  modulated intensity with a maximum at  $L \sim 0.5$ . The  $L$  modulated intensity of the spin resonance and our RPA calculations indicate that the superconducting gaps regarding the  $\alpha$  and  $\beta$  sheets have horizontal line nodes.

The experiments at AMATERAS were conducted under the J-PARC MLF user program with the proposal numbers 2018A0060 and 2018AU1402. The present work was supported by JSPS KAKENHI Grant Numbers JP17K05553 and JP17K14349, and the Cooperative Research Program of “Network Joint Research Center for Materials and Devices” (20181072).

\* k'iida@cross.or.jp

<sup>1</sup> Y. Maeno, H. Hashimoto, K. Yoshida, S. Nishizaki, T. Fujita, J. G. Bednorz, and F. Lichtenberg, *Nature (London)* **372**, 532–534 (1994).

<sup>2</sup> T. M. Rice and M. Sigrist, *J. Phys. Condens. Matter* **7**, L643 (1995).

<sup>3</sup> G. Baskaran, *Physica B* **223–224**, 490 (1996).

<sup>4</sup> A. P. Mackenzie and Y. Maeno, *Rev. Mod. Phys.* **75**, 657 (2003).

<sup>5</sup> Y. Maeno, S. Kitaoka, T. Nomura, S. Yonezawa, and K. Ishida, *J. Phys. Soc. Jpn.* **81**, 011009 (2012).

<sup>6</sup> K. Ishida, H. Mukuda, Y. Kitaoka, K. Asayama, Z. Q. Mao, Y. Mori, and Y. Maeno, *Nature (London)* **396**, 658–660 (1998).

<sup>7</sup> J. A. Duffy, S. M. Hayden, Y. Maeno, Z. Mao, J. Kulda, and G. J. McIntyre, *Phys. Rev. Lett.* **85**, 5412–5415 (2000).

<sup>8</sup> G. M. Luke, Y. Fudamoto, K. M. Kojima, M. L. Larkin, J. Merrin, B. Nachumi, Y. J. Uemura, Y. Maeno, Z. Q. Mao,

- Y. Mori, H. Nakamura, and M. Sigrist, *Nature (London)* **394**, 558-561 (1998).
- <sup>9</sup> J. Xia, Y. Maeno, P. T. Beyersdorf, M. M. Fejer, and A. Kapitulnik, *Phys. Rev. Lett.* **97**, 167002 (2006).
  - <sup>10</sup> J. R. Kirtley, C. Kallin, C. W. Hicks, E.-A. Kim, Y. Liu, K. A. Moler, Y. Maeno, and K. D. Nelson, *Phys. Rev. B* **76**, 014526 (2007).
  - <sup>11</sup> S. Yonezawa, T. Kajikawa, and Y. Maeno, *Phys. Rev. Lett.* **110**, 077003 (2013).
  - <sup>12</sup> S. Kittaka, A. Kasahara, T. Sakakibara, D. Shibata, S. Yonezawa, Y. Maeno, K. Tenya, and K. Machida, *Phys. Rev. B* **90**, 220502(R) (2014).
  - <sup>13</sup> Y. Amano, M. Ishihara, M. Ichioka, N. Nakai, and K. Machida, *Phys. Rev. B* **91**, 144513 (2015).
  - <sup>14</sup> N. Kikugawa, T. Terashima, S. Uji, K. Sugii, Y. Maeno, D. Graf, R. Baumbach, and J. Brooks, *Phys. Rev. B* **93**, 184513 (2016).
  - <sup>15</sup> K. Machida and M. Ichioka, *Phys. Rev. B* **77**, 184515 (2008).
  - <sup>16</sup> C. W. Hicks, D. O. Brodsky, E. A. Yelland, A. S. Gibbs, J. A. N. Bruin, M. E. Barber, S. D. Edkins, K. Nishimura, S. Yonezawa, Y. Maeno, and A. P. Mackenzie, *Science* **344**, 283-285 (2014).
  - <sup>17</sup> A. Steppke, L. Zhao, M. E. Barber, T. Scaffidi, F. Jerzembeck, H. Rosner, A. S. Gibbs, Y. Maeno, S. H. Simon, A. P. Mackenzie, and C. W. Hicks, *Science* **355**, eaaf9398 (2017).
  - <sup>18</sup> C. A. Watson, A. S. Gibbs, A. P. Mackenzie, C. W. Hicks, and K. A. Moler, *Phys. Rev. B* **98**, 094521 (2018).
  - <sup>19</sup> M. E. Barber, A. S. Gibbs, Y. Maeno, A. P. Mackenzie, and C. W. Hicks, *Phys. Rev. Lett.* **120**, 076602 (2018).
  - <sup>20</sup> Y. Luo, A. Pustogow, P. Guzman, A. P. Dioguardi, S. M. Thomas, F. Ronning, N. Kikugawa, D. A. Sokolov, F. Jerzembeck, A. P. Mackenzie, C. W. Hicks, E. D. Bauer, I. I. Mazin, and S. E. Brown, *Phys. Rev. X* **9**, 021044 (2019).
  - <sup>21</sup> V. Sunko, E. A. Morales, I. Marković, M. E. Barber, D. Milosavljević, F. Mazzola, D. A. Sokolov, N. Kikugawa, C. Cacho, P. Dudin, H. Rosner, C. W. Hicks, P. D. C. King, and A. P. Mackenzie, *npj Quantum Materials* **4**, 46 (2019).
  - <sup>22</sup> Y.-S. Li, N. Kikugawa, D. A. Sokolov, F. Jerzembeck, A. S. Gibbs, Y. Maeno, C. W. Hicks, M. Nicklas, and A. P. Mackenzie, arXiv:1906.07597.
  - <sup>23</sup> A. Pustogow, Y. Luo, A. Chronister, Y.-S. Su, D. A. Sokolov, F. Jerzembeck, A. P. Mackenzie, C. W. Hicks, N. Kikugawa, S. Raghu, E. D. Bauer, and S. E. Brown, *Nature (London)* **574**, 72-75 (2019).
  - <sup>24</sup> K. Ishida, M. Manago, and Y. Maeno, arXiv:1907.12236.
  - <sup>25</sup> K. Ishida, H. Mukuda, Y. Kitaoka, Z. Q. Mao, Y. Mori, and Y. Maeno, *Phys. Rev. Lett.* **84**, 5387-5390 (2000).
  - <sup>26</sup> I. Bonalde, B. D. Yanoff, M. B. Salamon, D. J. Van Harlingen, E. M. E. Chia, Z. Q. Mao, and Y. Maeno, *Phys. Rev. Lett.* **85**, 4775-4778 (2000).
  - <sup>27</sup> E. Hassinger, P. Bourgeois-Hope, H. Taniguchi, S. René de Cotret, G. Grissonnanche, M. S. Anwar, Y. Maeno, N. Doiron-Leyraud, and L. Taillefer, *Phys. Rev. X* **7**, 011032 (2017).
  - <sup>28</sup> S. Kittaka, S. Nakamura, T. Sakakibara, N. Kikugawa, T. Terashima, S. Uji, D. A. Sokolov, A. P. Mackenzie, K. Irie, Y. Tsutsumi, K. Suzuki, and K. Machida, *J. Phys. Soc. Jpn.* **87**, 093703 (2018).
  - <sup>29</sup> K. Machida, K. Irie, K. Suzuki, H. Ikeda, and Y. Tsutsumi, *Phys. Rev. B* **99**, 064510 (2019).
  - <sup>30</sup> I. I. Mazin and D. J. Singh, *Phys. Rev. Lett.* **82**, 4324 (1999).
  - <sup>31</sup> Y. Sidis, M. Braden, P. Bourges, B. Hennion, S. NishiZaki, Y. Maeno, and Y. Mori, *Phys. Rev. Lett.* **83**, 3320-3323 (1999).
  - <sup>32</sup> K. Iida, M. Kofu, N. Katayama, J. Lee, R. Kajimoto, Y. Inamura, M. Nakamura, M. Arai, Y. Yoshida, M. Fujita, K. Yamada, and S.-H. Lee, *Phys. Rev. B* **84**, 060402(R) (2011).
  - <sup>33</sup> S. Kunkemöller, P. Steffens, P. Link, Y. Sidis, Z. Q. Mao, Y. Maeno, and M. Braden, *Phys. Rev. Lett.* **118**, 147002 (2017).
  - <sup>34</sup> M. Braden, Y. Sidis, P. Bourges, P. Pfeuty, J. Kulda, Z. Mao, and Y. Maeno, *Phys. Rev. B* **66**, 064522 (2002).
  - <sup>35</sup> P. Steffens, Y. Sidis, J. Kulda, Z. Q. Mao, Y. Maeno, I. I. Mazin, and M. Braden, *Phys. Rev. Lett.* **122**, 047004 (2019).
  - <sup>36</sup> D. K. Morr, P. F. Trautman, and M. J. Graf, *Phys. Rev. Lett.* **86**, 5978 (2001).
  - <sup>37</sup> H. Suderow, V. Crespo, I. Guillamon, S. Vieira, F. Servant, P. Lejay, J. P. Brison, and J. Flouquet, *New J. Phys.* **11**, 093004 (2009).
  - <sup>38</sup> S. I. Ikeda, U. Azuma, N. Shirakawa, Y. Nishihara, and Y. Maeno, *J. Cryst. Growth* **237-239**, 787-791 (2002).
  - <sup>39</sup> Z. Q. Mao, Y. Maeno, and H. Fukazawa, *Mater. Res. Bull.* **35**, 1813 (2000).
  - <sup>40</sup> K. Nakajima, S. Ohira-Kawamura, T. Kikuchi, M. Nakamura, R. Kajimoto, Y. Inamura, N. Takahashi, K. Aizawa, K. Suzuya, K. Shibata, T. Nakatani, K. Soyama, R. Maruyama, H. Tanaka, W. Kambara, T. Iwashita, Y. Itoh, T. Osakabe, S. Wakimoto, K. Kakurai, F. Maekawa, M. Harada, K. Oikawa, R. E. Lechner, F. Mezei, and M. Arai, *J. Phys. Soc. Jpn.* **80**, SB028 (2011).
  - <sup>41</sup> Y. Inamura, T. Nakatani, J. Suzuki, and T. Otomo, *J. Phys. Soc. Jpn.* **82**, SA031 (2013).
  - <sup>42</sup> H. Iwasawa, Y. Yoshida, I. Hase, S. Koikegami, H. Hayashi, J. Jiang, K. Shimada, H. Namatame, M. Taniguchi, and Y. Aiura, *Phys. Rev. Lett.* **105**, 226406 (2010).
  - <sup>43</sup> T. Nagata, M. Urata, H. Kawano-Furukawa, H. Yoshizawa, H. Kadowaki, and P. Dai, *Phys. Rev. B* **69**, 174501 (2004).
  - <sup>44</sup> P. Blaha, K. Schwarz, G. K. H. Madsen, D. Kvasnicka, and J. Luitz, *Wien2k: An Augmented PlaneWave + Local Orbitals Program for Calculating Crystal Properties (Vienna University of Technology, Wien, 2001)*. (<http://www.wien2k.at/>)
  - <sup>45</sup> N. Marzari, A. A. Mostofi, J. R. Yates, I. Souza, and D. Vanderbilt, *Rev. Mod. Phys.* **84**, 1419-1475 (2012).
  - <sup>46</sup> J. P. Perdew, K. Burke, and M. Ernzerhof, *Phys. Rev. Lett.* **77**, 3865-3868 (1996).
  - <sup>47</sup> K. Suzuki, H. Usui, K. Kuroki, and H. Ikeda, *Phys. Rev. B* **96**, 024513 (2017).
  - <sup>48</sup> I. Žutić and I. Mazin, *Phys. Rev. Lett.* **95**, 217004 (2005).
  - <sup>49</sup> S. Kashiwaya, K. Saitoh, H. Kashiwaya, M. Koyanagi, M. Sato, K. Yada, Y. Tanaka, and Y. Maeno, *Phys. Rev. B* **100**, 094530 (2019).
  - <sup>50</sup> M. Braden, W. Reichardt, Y. Sidis, Z. Mao, and Y. Maeno, *Phys. Rev. B* **76**, 014505 (2007).